NICOLAUS COPERNICUS UNIVERSITY IN TORUŃ

Bulletin of Geography. Physical Geography Series, No. 31 (2026): 67–88
http://doi.org/10.12775/bgeo-2026-0011

Elevation-moderated thermal controls on Snow Melt Sensitivity: a remote sensing-based SMSI framework for Gulmarg in Jammu and Kashmir, India

Alok Kumar Dubey[1][a*], **Shalu Sinha**[2]

[1,2]Central University of South Bihar, Department of Development Studies, Daudnagar Gaya, Tekari, India

E-mail: alokdubey271504@gmail.com

[a] https://orcid.org/0000-0002-1100-8564

Abstract. Snowmelt conditions in high-altitude environments are increasingly influenced by rising temperatures, changing climatic conditions and local topography. The present study develops a multispectral geospatial framework to draw a Snow Melt Sensitivity Index (SMSI) for the Gulmarg region of Jammu and Kashmir using Landsat-9 OLI/TIRS and SRTM-DEM datasets. Four multispectral snow indices, namely Normalised Difference Snow Index (NDSI), Normalised Difference Snow-Cover Index (NDSCI), Normalised Difference Snow Moisture Index (NDSMI) and Snow Wetness Index (SWI) were integrated with Land Surface Temperature (LST) and elevation data. All variables were standardised using Z-score normalisation and weighted objectively through Principal Component Analysis (PCA). SMSI classification indicates that 67.79% of the region falls under moderate melt sensitivity, while 16.54% lies in high to very high sensitivity zones, primarily below 3,000 m elevation. Strong positive correlation between LST and SMSI (r=0.72) confirms thermal dominance in melt processes. The findings highlight elevation-moderated thermal control over snow dynamics and provide a robust framework for climate-sensitive mountain hydrology assessment.

Key words:
Snow Cover,
Melting Sensitivity,
Himalaya,
LST,
Elevation,
India

Introduction

The study of snowmelt dynamics in high-altitude mountainous environments has transitioned from a niche meteorological interest to a critical priority in global climate research. As the Earth undergoes unprecedented warming, the cryosphere stands as the most sensitive indicator of environmental change (Brahmbhatt et al. 2012; Joshi et al. 2015). In the Western Himalayas, specifically within the Pir Panjal range that cradles the Gulmarg region, the seasonal accumulation and subsequent depletion of snow cover serve as the primary regulator of regional hydrology, ecology and socio-economic stability (Vinze and Azam 2023; Bhat et al. 2025). For tourism, the ski-based winter industry in the Gulmarg region is highly sensitive to snow duration and depth, so shortened snow seasons and increased mid-winter melt led to reduced ski days, operational uncertainty and economic losses for local communities dependent on winter sports and snow-based recreation (Steiger et al. 2019; Sinha et al. 2025).

The global snow cover has been declining over recent decades. Over the period 2000–2022, annual snow cover declined by an average of 5.12%, with decreases exceeding increases two- to ten-fold, depending on the season and region studied (Young 2023). Long-term records indicate a negative trend in snow cover extent and duration, with trends such as a –3.6% per decade decrease in yearly snow cover extent and a shortening of snow cover duration by 15 days over recent decades (Notarnicola 2022).

The acceleration of snowmelt, driven by rising land surface temperature (LST) and altered precipitation patterns, is no longer a localised

© Author(s) 2026. This work is distributed under the Creative Commons Attribution 4.0 License (http://creativecommons.org/licenses/by-nc-nd/4.0/).

phenomenon. It is a cascading crisis affecting the cryosphere, tourism-dependent livelihoods and agricultural water security (Shafiq et al. 2019). In the Jammu and Kashmir region, a steady warming trend of ~0.0016°C per year has been identified over a five-decade period (Bhat et al. 2025). Snowmelt also aggravates natural disaster risks in the form of wet-snow and glide avalanches on steep slopes. Furthermore, Glacial Lake Outburst Floods (GLOFs) represent a significant threat, where rapid melting and ice-dam failure can generate high-magnitude flood waves threatening infrastructure and settlements (Dar et al. 2024).

Monitoring these complex cryospheric processes requires methodologies that can navigate the physical inaccessibility and harsh conditions of the high Himalayas. Remote sensing (RS) and Geographic Information System (GIS) have emerged as the most suitable tools for such studies due to their inherent advantages in cost-effectiveness, time efficiency and wide-area coverage (Taylor et al. 2021). Modern platforms such as Landsat-9, MODIS and Sentinel-2 offer a wide range of spectral bands that allow for the calculation of advanced indices. These include the Normalised Difference Snow Index (NDSI), the Normalised Difference Snow-Cover Index (NDSCI), the Snow Wetness Index (SWI) and the Normalised Difference Snow Moisture Index (NDSMI), which are essential for quantifying the sensitivity of snowmelt to climatic forcing. NDSI exploits high snow reflectance in the green band and strong SWIR absorption to map snow presence; NDSCI uses the NIR-SWIR contrast to improve discrimination of snow from other bright mountain surfaces; NDSMI is sensitive to changes in snow moisture because liquid water modifies NIR and SWIR2 reflectance; and SWI emphasises wetness or near-melting snow conditions through the SWIR/NIR relationship.

Against this backdrop, the Snow Melt Sensitivity Index (SMSI) provides an integrated framework to map how different terrain units in the Gulmarg region respond to thermal forcing. By integrating multi-spectral indices with LST modelling, it becomes possible to analyse snowmelt sensitivity with high accuracy. This framework can systematically identify zones of snowmelt sensitivity. This high vulnerability supports avalanche hazard assessments and informs adaptive management of water resources in a warming Himalayan climate.

Literature review

The cryosphere, comprising the Earth's frozen water components, is widely recognised as the most sensitive indicator of global climate oscillations. Within this context, the Himalayan mountain system, often referred to as the "Third Pole", is experiencing warming rates higher than the global average (Steger et al., 2013; Thiebault and Young, 2020). Research in the Western Himalayas and the Pir Panjal range has documented a significant shift in snowmelt dynamics, where the timing and volume of runoff are increasingly decoupled from historical norms (Garg et al. 2014). This transition is not merely meteorological; it is a cascading crisis affecting regional hydrology, biodiversity and the socio-economic stability of communities dependent on winter tourism and agriculture (Vinze and Azam 2023).

Traditionally, NDSI has been the "gold standard" for mapping snow-covered extent (Saloranta et al. 2019). However, recent studies argue that mapping snow extent is insufficient for understanding melt sensitivity. Modern research has shifted toward multi-spectral indices that characterise the internal physical state of the snowpack. Snow purity and compaction indices are used to identify the presence of light-absorbing impurities like black carbon/dust, which lowers albedo and accelerates melt (Dixit et al. 2019; Stillinger et al. 2023).

LST serves as the primary driver of the energy balance at the snow–atmosphere interface. Studies in the Indian Himalaya consistently show a strong negative correlation (ranging from −0.7 to −0.9) between temperature and snow water equivalent (Singh et al. 2012). LST is critical because it integrates both radiative and turbulent heat exchanges. Analysis in the Tien Shan Mountains demonstrated that LST, alongside elevation, explains the vast majority of spatial variability in snow consumption during peak ablation (Li et al. 2022). Although early literature treated the LST–snow relationship as linear, contemporary critical analysis, e.g., Haq et al. (2020) suggests a non-linear threshold effect. Once LST crosses a specific thermal threshold, the rate of melt accelerates exponentially due to the liquid water content in the snow. Furthermore, the interaction between LST and surface albedo creates a positive feedback loop: as LST rises, snow melts, exposing darker surfaces that absorb more radiation, further driving up LST. Integrated approaches that couple LST with multi-spectral snow indices provide a more process-oriented view of snowmelt sensitivity. In recent work on high-elevation Himalayan terrain, NDSCI, NDSMI and SWI provide additional diagnostic information on snow-cover purity, moisture

and wetness, which are important indicators of melt readiness and albedo reduction (Bormann et al. 2018; Dixit et al. 2019; Varade and Dikshit 2020; Husain et al. 2022; Stillinger et al. 2023).

Elevation fundamentally structures the environment in which snow persists. The concept of Elevation-Dependent Warming suggests that higher altitudes may experience more rapid warming than lowlands due to various feedback mechanisms (Desinayak et al. 2022). Himalayan studies show that temperature lapse rates are seasonally variable, steep during winter (~7°C per 1,000 m) and weaker during the monsoon (~2–3°C per 1,000 m), implying that modest vertical differences can lead to large contrasts in surface temperature and thus in snow persistence during the cold season (Kulkarni et al. 2007). Hypsographic analyses in the Hindu Kush Himalaya have revealed that snow cover decline is not uniform; specific elevation bands (e.g., 4,000–4,500 m) show more significant depletion than others, indicating "melt hotspots" where the climate sensitivity of the snowpack is at its peak (Stigter et al. 2016).

Research gap

Existing studies predominantly concentrate either on mapping snow-covered areas or basin-scale runoff modelling (Singh et al. 2012; Shafiq et al. 2019; Dimri et al. 2022; Poussin et al. 2023; Czapla-Myers et al. 2024). Studies have shown changes in snow cover and how it relates to NDVI and LST (Dixit et al. 2019; Shafiq et al. 2019; Haq et al. 2020; Dimri et al. 2022). A few studies look at LST and elevation separately instead of combining them into a single SMSI (Salomonson and Appel 2004; Stigter et al. 2016; Thiebault and Young 2020). There is currently no method of quantifying pixel-level snowmelt sensitivity that jointly incorporates spectral snow properties, LST and topography. They seldom use multi-spectral indices to show snow quality, moisture and wetness, nor do they turn these into clear sensitivity categories. Consequently, there is a clear gap in systematically analysing snowmelt sensitivity in the Gulmarg region using a full suite of multi-spectral snow indices rigorously derived from LST and detailed elevation data.

Objectives

The primary objective of the study is to develop an SMSI framework for Gulmarg using Landsat-9 multispectral/thermal data and SRTM-DEM topographic information.

The primary objective is subdivided into the following secondary objectives: (I) to derive NDSI, NDSCI, NDSMI and SWI and estimate LST from Landsat-9 data; (II) examine the influence of elevation and LST on spatial snowmelt sensitivity; (III) analyse correlations between LST and multispectral snow indices; (IV) generate SMSI using Z-score normalisation and PCA (Principal Component Analysis)-based weighting.

Profile of study area

The Gulmarg region is a primary study area within the Kashmir Valley, situated at an altitude of ~2,719 metres above mean sea level in the Pir Panjal mountain range of the inner Himalayas. The location of the study area is presented in Figure 2. The physiography of the Gulmarg sub-basin encompasses an area of 1,461 km^2 with a mean elevation of 3,034 m, a forest cover of 248.3 km^2, and a permanent glaciated area of 18 km^2. Topographic analysis reveals that 50% of the region lies between 3,000 m and 4,000 m altitude, while 74% of the ground cover is forested. The terrain is characterised by a predominantly northern aspect (53%) and slopes ranging between 15° and 30° across 44% of the area. This region experiences 48 average snowfall days annually, with maxima in February (14 days) and January (11 days) (Sharma et al. 2012; Misra et al. 2020; Rafiq et al. 2021). Meteorological data for the basin is monitored by an observatory at an altitude of 2,823 m. The Pir Panjal range, which divides the Kashmir Valley from the outer Himalayas, extends from east-south-east to west-north-west across Jammu and Kashmir and Himachal Pradesh, measuring ~2,621 km in length and 50 km in breadth. Globally recognised for its tourism, the charm of the region is deeply rooted in its snowfall, which serves as a major source of supply for the River Jhelum. A total of 66% of the discharge of the river is contributed by snowmelt, with annual stream flow contributions from snow and glacier melt reaching 33% in early spring, 73% in late spring and 68% during the summer (Jeelani et al. 2012). This water is critical for regional irrigation and the generation of hydropower. According to Figure 1, the annual mean temperature in Gulmarg shows a strong increasing trend over the last decade, with a slope of 0.73°C per year, indicating rapid warming. Despite interannual fluctuations, the overall trajectory is clearly upward, especially after 2019. The sharp rise from earlier low values to consistently

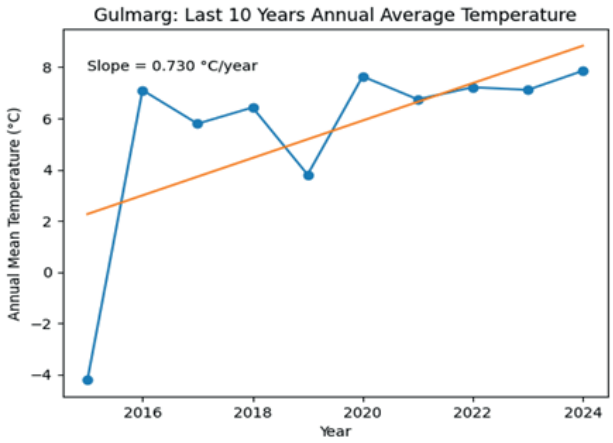

Fig. 1. Annual Mean Temperature in Gulmarg

warmer years suggests intensified thermal conditions in recent years. This accelerated warming trend may significantly enhance snow melt sensitivity and reduce snow persistence at higher elevations.

Description of dataset

Multispectral satellite data have been used in this study, which was acquired from Landsat-9 Operational Land Imager and Thermal Infrared Sensor (OLI/TIRS) on 4 February, 2025. The western disturbances bring heavy precipitation during the winter months from November to April. The month-wise average snowfall days are maximum in February; hence, the snow cover extent is also maximum during this month (Negi et al. 2009;

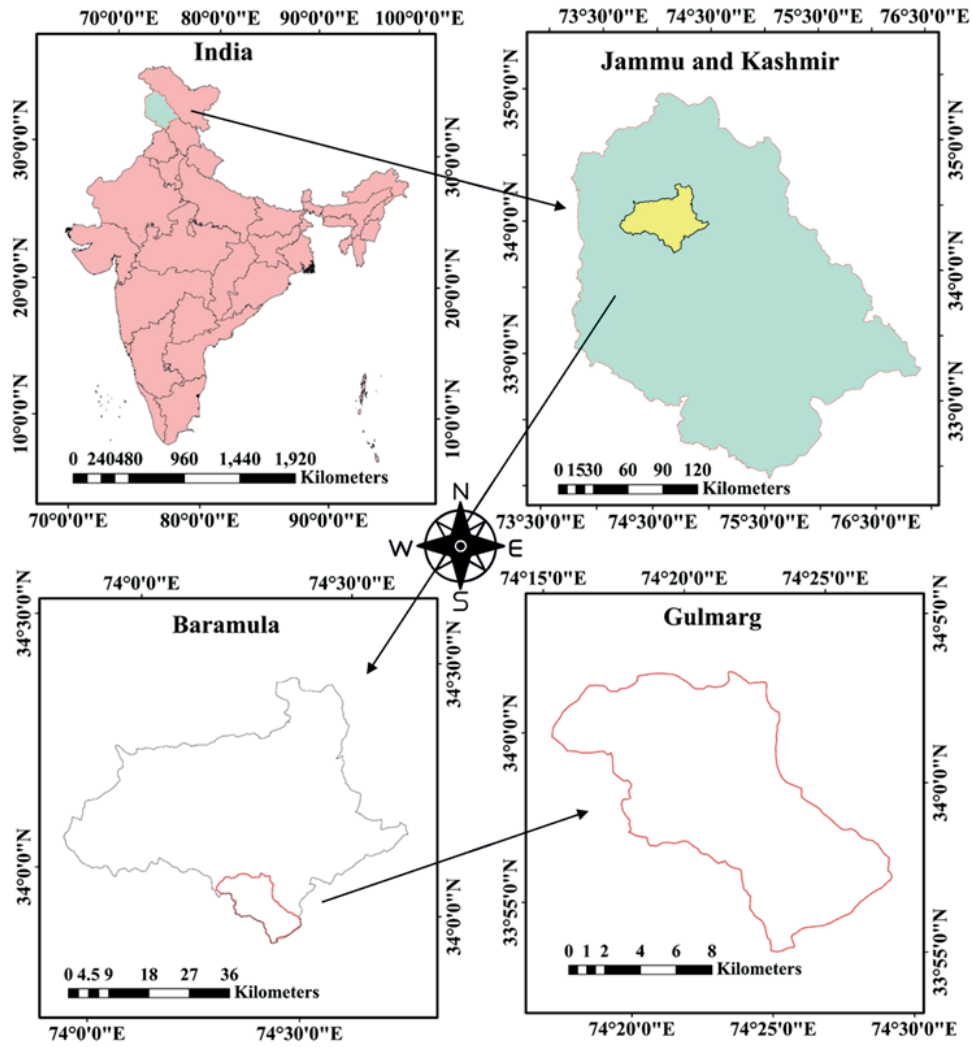

Fig. 2. Location of the study area

Citation: Bulletin of Geography. Physical Geography Series 2026, 31, http://doi.org/10.12775/bgeo-2026-0011

Mishra and Rafiq 2017; Rafiq et al. 2021). Therefore, the selection of the date is based on minimal cloud cover (<5%) over the study area. The dataset was downloaded from an open-access website, the United States Geological Survey Earth Explorer portal (https://earthexplorer.usgs.gov/). The imagery corresponds to Path/Row of 149/037 and is projected in the Universal Transverse Mercator (UTM) projection, Zone 43N. It referenced the WGS 1984 datum. The visible, NIR and SWIR OLI bands have 30 m spatial resolution and were used for snow-index computation. The Landsat-9 TIRS thermal bands are originally acquired at 100 m spatial resolution and are resampled to 30 m in Collection 2 products; therefore, although the LST layer is spatially aligned with 30 m optical bands, its effective thermal detail remains coarser than the VIS/NIR/SWIR information. The topographic information was obtained from the Shuttle Radar Topography Mission Digital Elevation Model (SRTM-DEM) at 30 m spatial resolution. The SRTM-DEM was used to examine altitudinal controls on snow distribution and land surface temperature. The DEM was resampled and spatially aligned with the Landsat-9 data to ensure pixel-level consistency before integrated analysis. Table 1 contains all the essential information of dataset.

Pre-processing of data

The transformation of raw satellite data into geophysical meaningful parameters begins with the radiometric calibration and atmospheric restoration. Digital number (DN) values of the required bands of the Landsat-9 imagery were converted into Top-of-Atmosphere (TOA) spectral radiance and reflectance using radiometric rescaling coefficients provided in the metadata file (Yin et al. 2022; Trevisiol et al. 2024). This step was taken to ensure the comparability of spectral information across bands and scenes. Following the radiometric calibration, the atmospheric correction is performed to derive the Bottom-of-Atmosphere (BOA) surface reflectance (Gross et al. 2022; Choate et al. 2023). This step is critical because the atmospheric dust particles and aerosols can scatter and absorb radiation, which may affect the derivation of snow-related spectral indices and LST. However, snow and ice surfaces pose specific atmospheric-correction challenges because their high visible reflectance, anisotropic reflectance behaviour, topographic illumination effects and potential adjacency effects differ from vegetation or bare-soil targets. Accordingly, the above-mentioned corrections were considered appropriate for a regional-scale SMSI assessment, similarly used in the other studies. The uncertainty over bright snow and mixed terrain is also explicitly acknowledged. The clouds, cloud shadow and snow cloud confusion were addressed using the Quality Assessment (QA) bands and index-based thresholding techniques (Voskanian et al. 2023; Czapla-Myers et al. 2024). The pixels affected by clouds and shadows were masked out to avoid the contamination of the calculation of the spectral indices and LST.

Table 1. Description of the dataset

Sr. No.	Parameter	Description
1.	Date	04-02-2025
2.	Map projection	UTM
3.	UTM Zone	43N
4.	Datum	WGS1984
5.	Projection unit	Meter
6.	Pixel area	(100m×100m for thermal bands) 30m×30m for other bands
7.	Number of bands	11
8.	Path/Row	149/037
9.	Satellite	Landsat-9
10.	Sensor	OLI/TIRS
11.	Source	https://earthexplorer.usgs.gov/

Methods

This section sequentially presents the calculation of all spectral indices, LST and elevation from satellite data. Additionally, it explains the integration of all layers to analyse the SMSI. All the steps are represented in Figure 3.

Calculation of multispectral snow indices

A total of four snow indices has been calculated to ensure the higher accuracy and robustness of the model. The purpose and equation for the calculation of all multispectral snow indices are given in Table 2. The higher NDSI values indicate the presence of snow cover in the area, while lower or negative values represent snow-free surfaces like vegetation cover, barren land, built-up

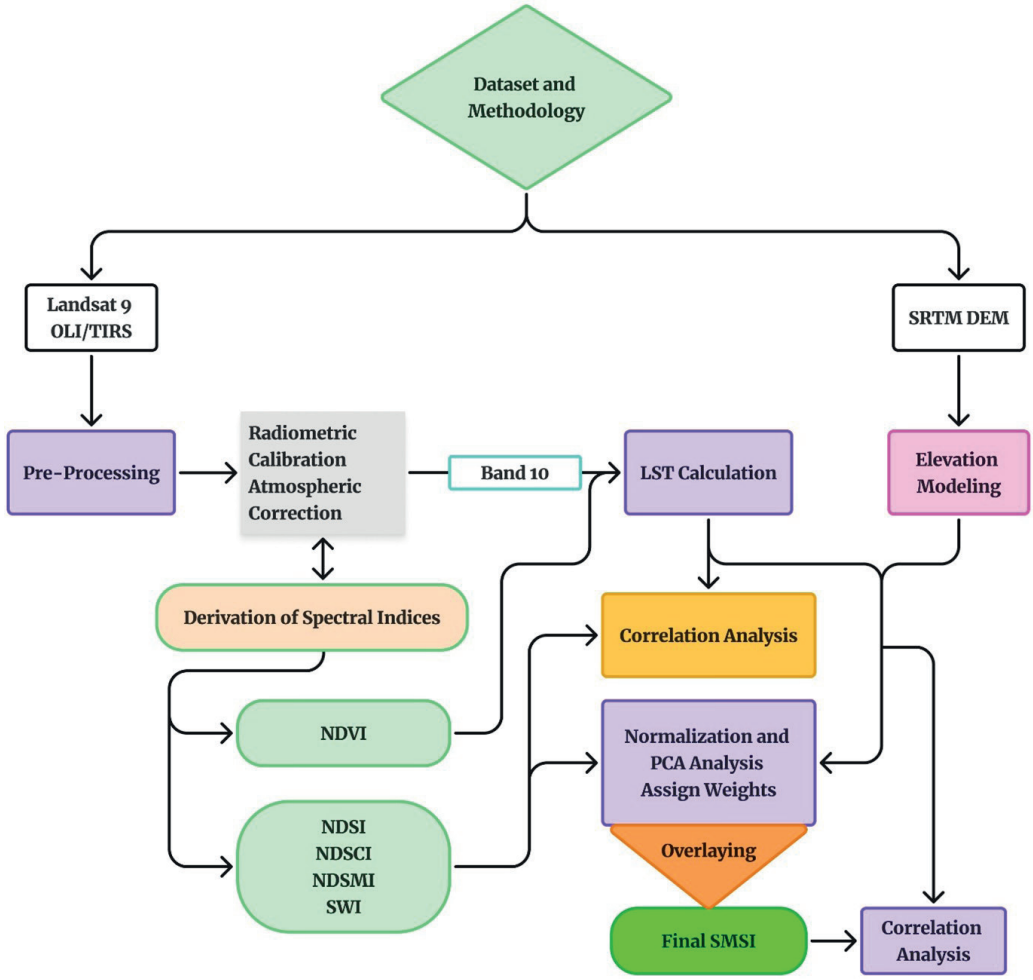

Fig. 3. Study methodology

Table 2. Derivation of the multispectral snow indices

Sr. No.	Spectral indices	Purpose	Equation	Bands in Landsat-9	References
1.	Normalised Difference Snow Index (NDSI)	Indicates the presence of snow cover in the area	(Green - SWIR) / (Green + SWIR)	Green = Band 3; SWIR (Short Wave Infrared) = Band 6	(Dixit et al. 2019a; Mudryk et al. 2017; Potopová et al. 2016; Raghubanshi et al. 2023; Satti et al. 2023; Zaz et al. 2018)
2.	Normalised Difference Snow-Cover Index (NDSCI)	Enhances discrimination between snow and other bright surfaces, e.g., clouds, exposed mountain rock	(NIR - SWIR) / (NIR + SWIR)	NIR (Near Infrared) = Band 5; SWIR = Band 6	
3.	Normalised Difference Snow Moisture Index (NDSMI)	Calculates moisture content within snowpack	(NIR - SWIR2) / (NIR + SWIR2)	NIR = Band 5; SWIR2 = Band 7	
4.	Snow Wetness Index (SWI)	Directly captures relative increase in liquid water within snowpack	SWIR / NIR	SWIR = Band 6; NIR = Band 5	

area or water surfaces (Singh et al. 2012). It exploits the high reflectance of snow in the visible green region and its strong absorption in the shortwave infrared region (Sharma et al. 2012). The NDSCI is calculated using the high reflectance of the NIR region and low reflectance in the SWIR region by the snow, making it effective for identifying persistent and pure snow cover (Gurung et al. 2017). In the NDSMI, the NIR region of the spectrum is strongly absorbed by the water within the snowpacks (Sharma et al. 2012; Huang et al. 2016). As the snow becomes wet, the absorption of the SWIR2 region increases strongly due to the water, because this spectrum region is more sensitive to liquid water content. The SWI quantifies the melting of near-melting conditions using the reflectance ratio of the SWIR to the NIR (Dixit et al. 2019). It also exploits the strong absorption of SWIR by the liquid water (Dar et al. 2014).

Snow cover extent analysis

The snow-covered and snow-free areas were delineated using the threshold-based classification of NDSI derived from the satellite data. A widely accepted threshold of NDSI>0.4 was applied to identify snow-covered pixels, while values of NDSI<0.4 were classified as snow-free surfaces. The same threshold method was applied in many cryospheric studies on the Himalayan region (Ma and Zhang 2022; Poussin et al. 2023). Additionally, the NDSCI was also used to minimise the confusion between the snow pixels and clouds and other bright surfaces (Oparin et al. 2014). This combined threshold approach enhanced the classification accuracy and ensured the reliable discrimination between the snow-covered and snow-free areas before further SMSI analysis.

Elevation analysis

The elevation analysis for the Gulmarg region was conducted using the SRTM-DEM data. Elevation is used as the primary topographic control because it directly influences air and surface temperature through lapse-rate effects, controls snow persistence, and structures the vertical distribution of accumulation and melt zones. Further, the hypsometric and area distribution analyses were performed to derive, respectively, the maximum, minimum and mean elevation and the area under each elevation class. The classified elevation zones were subsequently integrated with the final SMSI classes.

Calculation of LST

The LST was calculated from the thermal infrared band (band 10) of Landsat-9 data. The official Landsat Collection 2 Surface Temperature products were considered as a reference alternative; however, a custom LST derivation was retained to maintain methodological consistency with the selected optical preprocessing, masking and SMSI layer construction. LST was calculated using the following steps:

1. Conversion of DN to spectral radiance: The DN values of the pixels were converted into TOA spectral radiance using Equation 1 (Dubey et al. 2025).

$$L_\lambda = M_L \times Q_{cal} + A_L \quad (1)$$

Where, L_λ= TOA spectral radiance, M_L= Radiance multiplicative scaling factor (given in Metadata file), Q_{cal}= DN value pixels, A_L= Radiance additive scaling factor (given in Metadata file).

2. Conversion to brightness temperature (BT): The radiance values were converted to at-sensor brightness temperature using Planck's law, given as Equation 2 (Adeola Fashae et al. 2020).

$$T_B = \frac{K_2}{ln\left(\frac{K_1}{L_\lambda} + 1\right)} \quad (2)$$

Where, T_B= Brightness Temperature (BT) in Kelvin, K_1 and K_2= Thermal conversion constants (given in the Metadata file), L_λ= TOA spectral radiance.

3. Estimation of land surface emissivity (ε): Surface emissivity was estimated using the Normalised Difference Vegetation Index (NDVI) based method, because the Gulmarg contains heterogeneous mixtures of snow, exposed rock, forest, meadow and partially snow-covered pixels. It provides a practical approximation of emissivity for heterogeneous mountainous terrain. The NDVI was calculated using Equations 3, 4 and 5 (Panahi et al. 2013; Malik et al. 2019; Guha et al. 2020).

$$NDVI = \frac{(NIR - Red)}{(NIR + Red)} \quad (3)$$

Where, NIR = Band 5 and Red = Band 4 in Landsat-9 data.

$$Proportion of Vegetation(P_v) = \left(\frac{NDVI - NDVI_{min}}{NDVI_{max} - NDVI_{min}}\right)^2 \quad (4)$$

$$\varepsilon = 0.004 \times P_v + 0.986 \quad (5)$$

4. Final LST derivation: The final LST was derived using the following Equation 6 (Grover and Singh 2016; Wang et al. 2017; Sam and Balasubramanian 2023).

$$LST(K) = \frac{T_B}{1 + \left(\frac{\lambda T_B}{\rho}\right) \ln(\varepsilon)} \quad (6)$$

Where, LST (K) = Land surface temperature in Kelvin, T_B= Brightness temperature in Kelvin, λ= Effective wavelength of band 10, ρ=hc/σ (h= Plank's constant, c = speed of light, σ = Boltzmann constant), ε = Emissivity.

5. LST Kelvin to LST Celsius: Equation 7 was used to convert the derived LST from Kelvin to Celsius (Adeola Fashae et al. 2020).

$$LST\ (℃) = LST(K) - 273.15 \quad (7)$$

Correlation analysis

The Karl Pearson correlation coefficient was used in this study to quantify the linear relationship between LST and the multispectral snow indices (NDSI, NDSCI, NDSMI and SWI). Pearson correlation was selected to measure the strength and direction of linear association among continuous variables derived from satellite data (Blyth 1994; Akinkunmi and Etebefia 2019). Initially, the correlation analysis was conducted between LST and each of the multispectral snow indices to evaluate their thermal sensitivity. Subsequently, the analysis was extended to assess the combined influence of LST and elevation on the SMSI. This approach was used to determine whether SMSI is primarily thermally driven or controlled by topographic factors. The Karl Pearson correlation coefficient was computed using Equation (8):

$$rxy = \frac{\sum(X_i - \bar{X})(Y_i - \bar{Y})}{\sqrt{\sum(X_i - \bar{X})^2 \sum(Y_i - \bar{Y})^2}} \quad (8)$$

Where X_i and Y_i represent paired observations of the two variables, $\bar{X}$ and $\bar{Y}$ denote their respective means and i is the total number of valid observations. The coefficient rranges between −1 and +1, where positive values indicate direct relationships, negative values indicate inverse relationships and values near zero suggest weak or no linear association.

Principal Component Analysis (PCA) to weigh the factors

The PCA method is used to assign the weights to all the multi-spectral indices, LST and elevation to SMSI. This method was applied through the following steps:

1. Data standardisation: All the input variables were standardised before assigning the weights to eliminate the differences in scale and unit. Since these variables represent different quantities, direct comparison is not statistically meaningful. The standardisation was performed using the Z-Score normalisation presented as the following Equation 9 (Rani et al. 2025).

$$Z_i = \frac{X_i - \mu_i}{\sigma_i} \quad (9)$$

Where, Z_i = Normalised value for the variable *i*, X_i = Original pixel value, μ_i = Mean value of that variable, σ_i = Standard deviation of that specific variable.

2. PCA loadings: The PCA was applied to the standardised dataset to objectively determine the contribution of each variable to the snow melt variability. The first principal component (PC1), which accounts for the highest proportion of the total variance, was selected for the weight extraction (Abdi and Williams 2010; Bro and Smilde 2014) because it presents the dominant environmental gradient influencing the snow melt sensitivity. The loading values obtained from PC1 indicate the relative contribution of each variable. Variables exhibiting higher absolute loading values exert greater influence on snow melt dynamics. The absolute value of the PC1 loadings was normalised

using the following Equation 10 to compute the proportional weights for each variable (Ringnér 2008):

$$w_i = \frac{|l_i|}{\sum |l_i|} \quad (10)$$

3. The weighted overlay for the final SMSI: The weighted overlay of all thematic layers was performed on ArcMap to construct an SMSI (Karimi et al. 2019). Before overlay, all the raster layers were reclassified to a common scale and resampled to a uniform spatial resolution to ensure pixel-level compatibility (Özkan et al. 2019; Dwivedi et al. 2024). The PCA-derived weights were assigned to each corresponding raster layer in the Weighted Overlay tool within the Spatial Analyst extension. The positive weights were assigned to variables directly related to melt sensitivity. The final SMSI raster was generated using a weighted linear combination approach, where each pixel value represents the cumulative influence of LST, multi-spectral snow indices and topographic factors on snow melt susceptibility (Olusina and Shyllon 2014; Oyedele et al. 2022; Devaki and Shanmugapriya 2023).

Results and discussion

Description of multi-spectral snow indices

The NDSI map (Fig. 4A) shows a strong dominance of high index values across the central zones, indicating widespread snow cover during the acquisition period. The index ranges from −0.0714 to 0.7472 (Table 3), with a relatively high mean value of 0.53 and standard deviation of 0.1229, suggesting substantial snow coverage with moderate spatial variability. Areas exhibiting lower or slightly negative

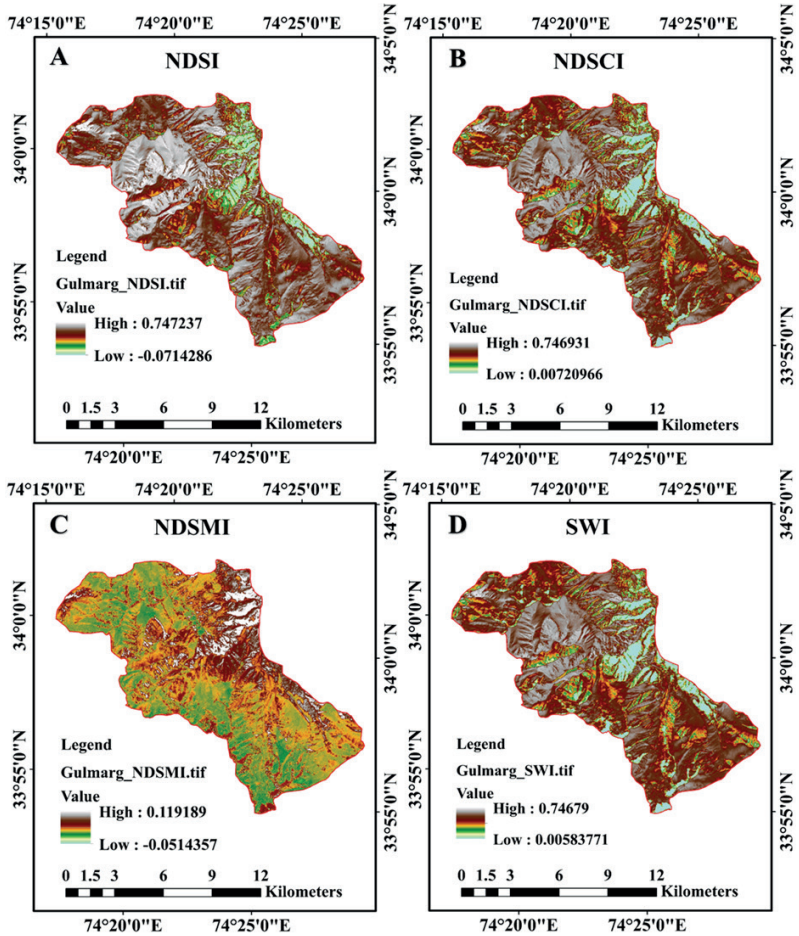

Fig. 4. Multi-Spectral Snow Indices (A: NDSI, B: NDSCI, C: NDSMI and D: SWI)

Table 3. Description of the multi-spectral snow indices

Sr. No	Snow Indices	Maximum	Minimum	Mean	Std.
1.	NDSI	0.7472	-0.0714	0.53	0.1229
2.	NDSCI	0.7469	0.0072	0.534	0.1289
3.	NDSMI	0.119	-0.051	-0.005	0.016
4.	SWI	0.746	0.005	0.531	0.124

values correspond to non-snow surfaces such as exposed rock, vegetation or mixed pixels. The high maximum value (0.7472) validates the presence of dense and relatively clean snowpack in the study area.

The NDSCI map (Fig. 4B) displays a spatial pattern closely aligned with NDSI, which is expected since both indices exploit SWIR absorption characteristics of snow. However, NDSCI shows slightly refined differentiation in ridge and slope regions, likely enhancing snow-cloud and snow-bright surface discrimination. According to Table 3, the index varies from 0.0072 to 0.7469, with a mean of 0.534 and a standard deviation of 0.1289, slightly higher than NDSI. This indicates marginally greater dispersion and improved sensitivity to surface snow condition. The absence of strongly negative values suggests more stable classification of snow-covered pixels and reduced misclassification of non-snow surfaces.

In contrast to NDSI and NDSCI, the NDSMI map (Fig. 4C) exhibits significantly lower magnitude values, ranging from –0.051 to 0.119, with a mean of –0.005 and a very low standard deviation of 0.016 (Table 3). This narrow value range indicates subtle spectral differences associated with internal snow moisture rather than snow presence. The spatial pattern shows a patchy distribution, particularly on south-facing slopes, where melt processes are more active. Positive and higher values suggest increasing liquid water content, indicating moist or melting snow conditions. The relatively small standard deviation confirms that moisture variation is less spatially dominant compared to overall snow extent.

The SWI map (Fig. 4D) demonstrates patterns similar to NDSI and NDSCI in terms of spatial distribution but reflects snow wetness dynamics more directly. The index ranges from 0.005 to 0.746, with a mean of 0.531 and standard deviation of 0.124, indicating moderate variability in snow wetness conditions. Higher SWI values are observed in lower and transitional elevation zones, consistent with melt-prone regions. Compared to NDSMI, SWI shows a broader dynamic range, making it more responsive to active melt processes.

Snow cover extent analysis

The classified Figure 5 indicates that ~76.22 km² (Table 4) of the study area is covered by snow, accounting for nearly 58.44% of the total area of Gulmarg. Snow cover is predominantly concentrated in the central and higher-altitude regions. These zones correspond to ridge tops, upper slopes and north-facing aspects, where snow accumulation and persistence are higher. In contrast, 54.20 km² (41.56%) of the area is snow-free, primarily in lower elevation zones, south-facing slopes and valley regions. These areas are more exposed to solar radiation and experience relatively

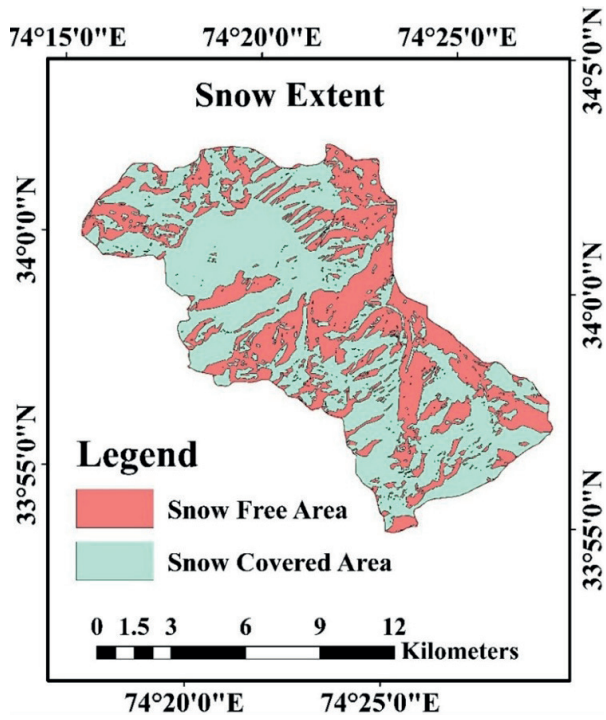

Fig. 5. Snow cover extent in Gulmarg

Table 4. Snow cover extent in Gulmarg

Sr. No.	Class	Area in km²	%
1.	Snow-covered area	76.22	58.44
2.	Snow-free area	54.20	41.56
3.	**Total**	**130.42**	**100**

Table 5. Description of the multi-spectral snow indices

Sr. No.	LST Parameter	Value in °C
1.	Maximum	12.92
2.	Minimum	-3.90
3.	Mean	4.59
4.	Standard Deviation	5.47

higher land surface temperatures, leading to reduced snow retention and increased melt activity.

Thermal dynamics of Gulmarg

The LST distribution across Gulmarg exhibits substantial spatial variability, with temperatures ranging from a minimum of −3.90°C to a maximum of 12.92°C. All the stats of LST are given in Table 5 and in Figure 6. The mean LST of 4.59°C indicates overall cool surface conditions during the observation period, consistent with the presence of widespread snow cover at higher elevations. The relatively high standard deviation of 5.47°C reflects pronounced spatial heterogeneity in surface temperature, likely influenced by elevation gradients, slope–aspect variations, land cover differences and snow distribution patterns. This marked thermal contrast highlights the strong topographic control on surface temperature and its critical role in regulating snow persistence and melt dynamics within the study area (Romshoo et al. 2014; Xu et al. 2017; Prakash and Norouzi 2020).

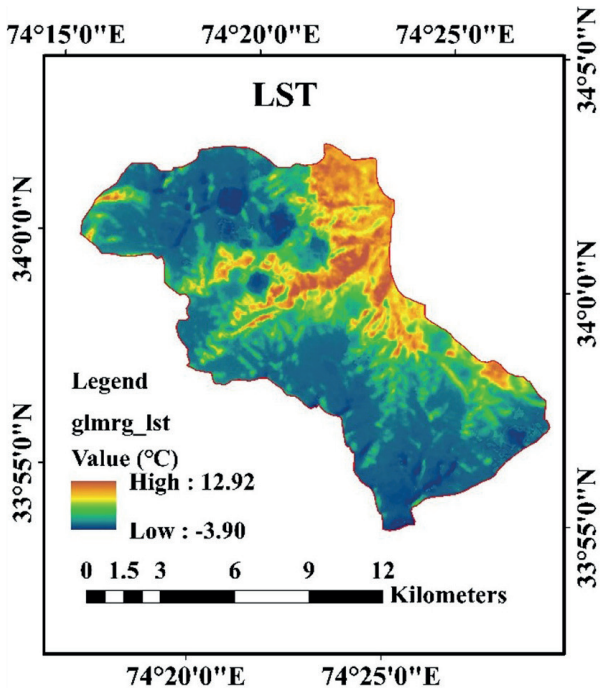

Fig. 6. Land Surface Temperature in Gulmarg

Correlation between LST and multi-spectral snow indices

The correlation analysis between LST and the multispectral snow indices is presented in Figure 7. It reveals statistically significant relationships ($p<0.001$) across all variables, highlighting strong thermal control on snow dynamics in Gulmarg. The relationship between LST and NDSI shows a strong negative correlation (R2=−0.61), indicating that higher snow cover values are associated with lower LST, which is physically consistent, as snow-covered areas exhibit lower thermal signatures due to high albedo and latent heat effects (Thiebault and Young 2020). Similarly, LST and NDSCI demonstrate a moderate negative correlation (R2=−0.47), suggesting that cleaner and more persistent snow cover corresponds to LST conditions, although the relationship is slightly weaker compared to NDSI. In contrast, LST exhibits a strong positive correlation with NDSMI (R2=0.61), implying that increasing LST enhances internal snow moisture and melt progression. A moderate positive correlation is also observed between LST and SWI (R2=0.52), confirming that snow wetness intensifies under warmer conditions (Rasul and Ningthoujam 2021). Overall, the negative correlations for NDSI and NDSCI and positive correlations for NDSMI and SWI collectively demonstrate that, with rising surface temperature, snow presence decreases while moisture and wetness increase, reinforcing the thermally driven nature of snow melt processes in the study area (Arekhi 2016; Husain et al. 2022).

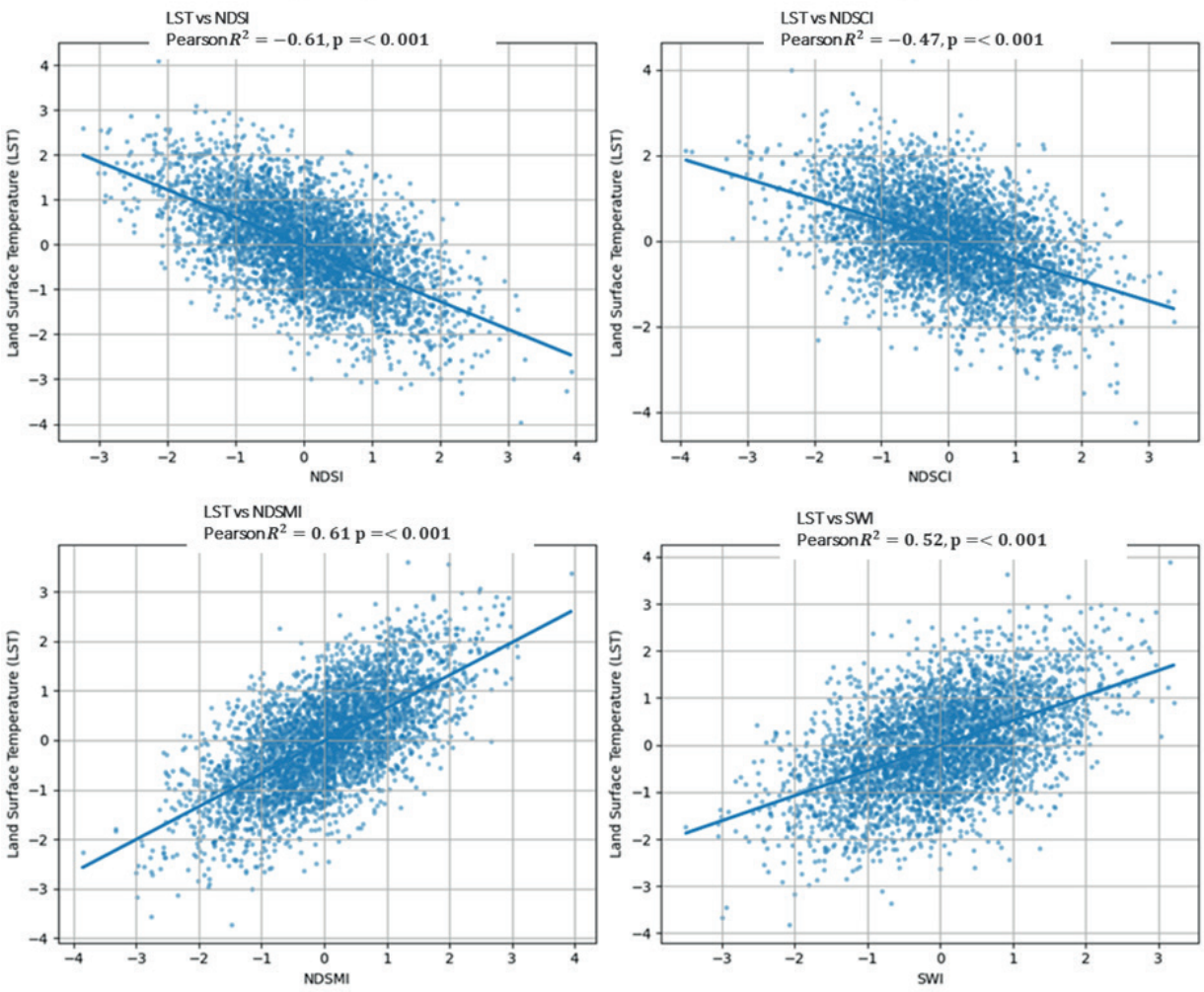

Fig. 7. Correlation between LST and Multi-Spectral Snow Indices

Elevation modelling of Gulmarg

Figures 8 and 9 represent the elevation map and elevation-area distribution profile of Gulmarg, respectively. The elevation profile of Gulmarg demonstrates pronounced topographic variability characteristic of high-altitude Greater Himalayan terrain (Steger et al. 2013). According to Table 6, elevation ranges from a minimum of 2,331 m to a maximum of 4,557 m, resulting in a substantial altitudinal range of 2,226 m across the study area. The mean elevation of 3,589.30 m indicates that the region is predominantly situated in a high-mountain environment, which strongly influences climatic conditions, snow accumulation and melt dynamics. The relatively moderate standard deviation of 408.41 metres reflects considerable but spatially structured variation in terrain, with steep gradients observed between ridge crests and valley bottoms (Steger et al. 2013). Higher elevations are concentrated along ridge systems and central mountainous zones, while comparatively lower elevations occur in valley corridors and peripheral slopes (Baba et al. 2019). This significant altitudinal contrast plays a critical role in regulating temperature distribution, snow persistence and moisture variability, reinforcing the importance of topographic control in the snow melt processes observed within the region.

Assigning weight to SMSI drivers

Since the selected variables (LST in°C, Elevation in metres, and snow indices as unitless ratios) are measured

Citation: Bulletin of Geography. Physical Geography Series 2026, 31, http://doi.org/10.12775/bgeo-2026-0011

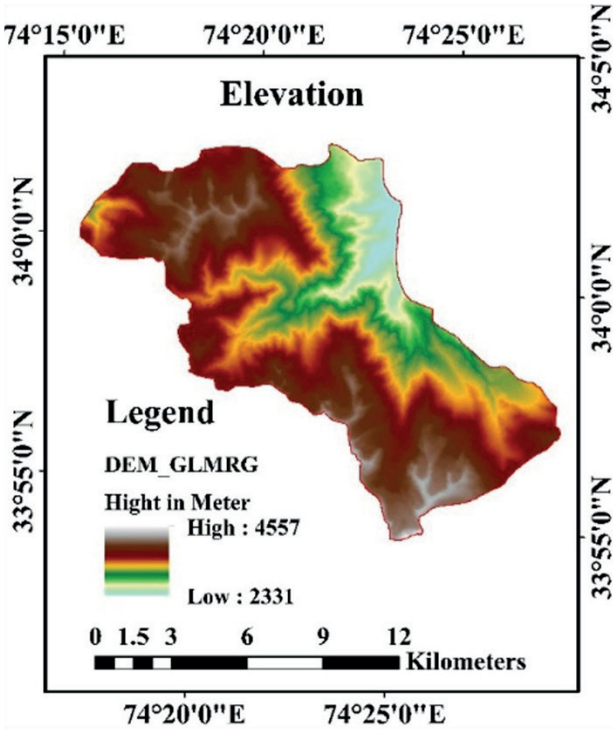

Fig. 8. Elevation modelling in Gulmarg

in different units and scales, direct comparison is not statistically appropriate. Therefore, all variables were standardised using Z-score normalisation method to remove scale effects and ensure comparability (Bro and Smilde 2014). After standardisation, the correlation matrix was computed. The correlation matrix represents the linear association between variables independent of their units. PCA was performed on this matrix instead of the covariance matrix to ensure equal weighting of scale (Abdi and Williams 2010; Shrestha 2021). PCA decomposes the correlation matrix into eigenvalues and eigenvectors. Each principal component represents a linear combination of the original variables. The first principal component (PC1) captures the maximum proportion of total variance. All the values of PC1 loading, absolute loading, final PCA weightage and weight in % for the overlaying are given in Table 7.

According to Table 7, the PCA results indicate that PC1 explains 55.77% of the total variance, reflecting a dominant environmental gradient controlling snow melt sensitivity in the Gulmarg region. Among the variables, LST exhibits the highest loading (0.536) and corresponding PCA weight of 0.246585 (24.7%),

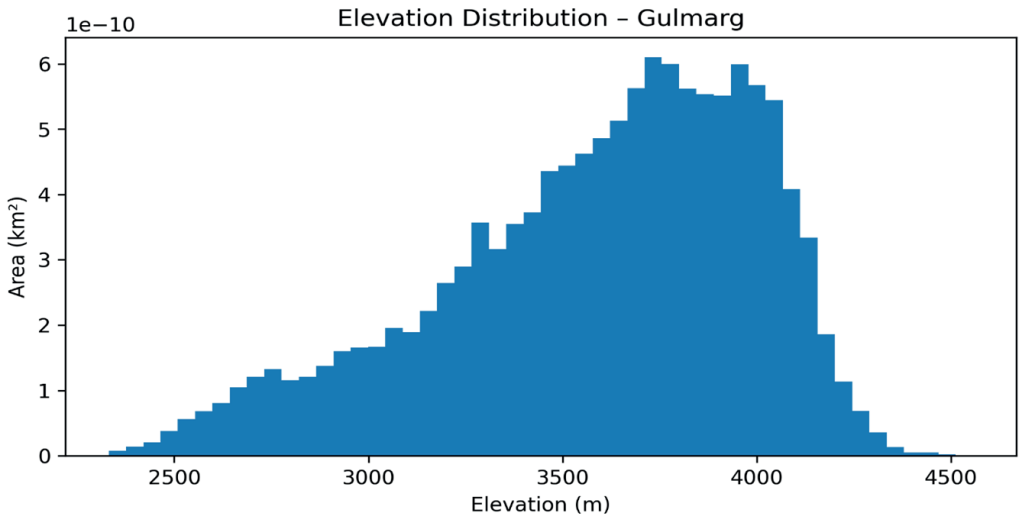

Fig. 9. Elevation and area distribution in Gulmarg

Table 6. Elevation in Gulmarg

Elevation parameter	Value in metres
Maximum	4,557
Minimum	2,331
Mean	3,589.30
Standard deviation	408.41

identifying it as the primary driver of melt processes. Elevation follows closely with a loading of 0.520 and a weight of 0.239122 (23.9%), highlighting strong topographic control through lapse-rate effects. The SWI also contributes substantially with a loading of 0.505119 and PCA weightage of 0.232218 (23.2%), suggesting that surface wetness conditions play a significant role in active melt dynamics. NDSMI shows a

Table 7. PCA weightage to the drivers

Variance Explained by PC1: 0.55774015				
Variable	**PC1 loading**	**Absolute loading**	**PCA weight**	**Weight in %**
LST	0.536372	0.536372	0.246585	24.7
Elevation	0.520138	0.520138	0.239122	23.9
SWI	-0.505119	0.505119	0.232218	23.2
NDSMI	-0.339028	0.339028	0.155861	15.6
NDSI	0.267636	0.267636	0.123040	12.3
NDSCI	0.006904	0.006904	0.003174	0.3

moderate influence with 0.339028 loading values and a weight of 0.155861 (15.6%), with its negative loading indicating an inverse relationship with the dominant gradient, although its magnitude confirms a meaningful contribution. With a loading of 0.267636 and PCA weightage of 0.123040 (12.3%), the NDSI contributes modestly, reflecting the secondary role of snow extent in determining melt sensitivity. In contrast, NDSCI has a negligible loading value of 0.006904 and PCA weight of 0.003174 (0.3%), indicating minimal influence on the dominant melt variability pattern. Overall, the table demonstrates that snow melt sensitivity is primarily thermally driven, strongly moderated by elevation and further influenced by wetness and moisture conditions, while snow cover conditions play an insignificant role (Tian et al. 2022).

Final SMSI analysis

The spatial distribution of the SMSI across the Gulmarg region reveals a pronounced altitudinal and thermal gradient controlling melt dynamics. Figure 10A shows the continuous SMSI index and Figure 10B highlights the SMSI classes across the Gulmarg region. According to Table 8, the moderate sensitivity class dominates the landscape, covering an area of 88.40 km^2 (67.79%), primarily between elevations of 3,000 m and 3,499 m and corresponding LST ranges of 5.34°C to 7.57°C. This indicates that nearly two thirds of the region exists in a transitional melt regime where snowpack conditions are neither completely stable nor undergoing extreme ablation (Brahmbhatt et al. 2012). Such mid-elevation zones are climatically sensitive and may respond rapidly

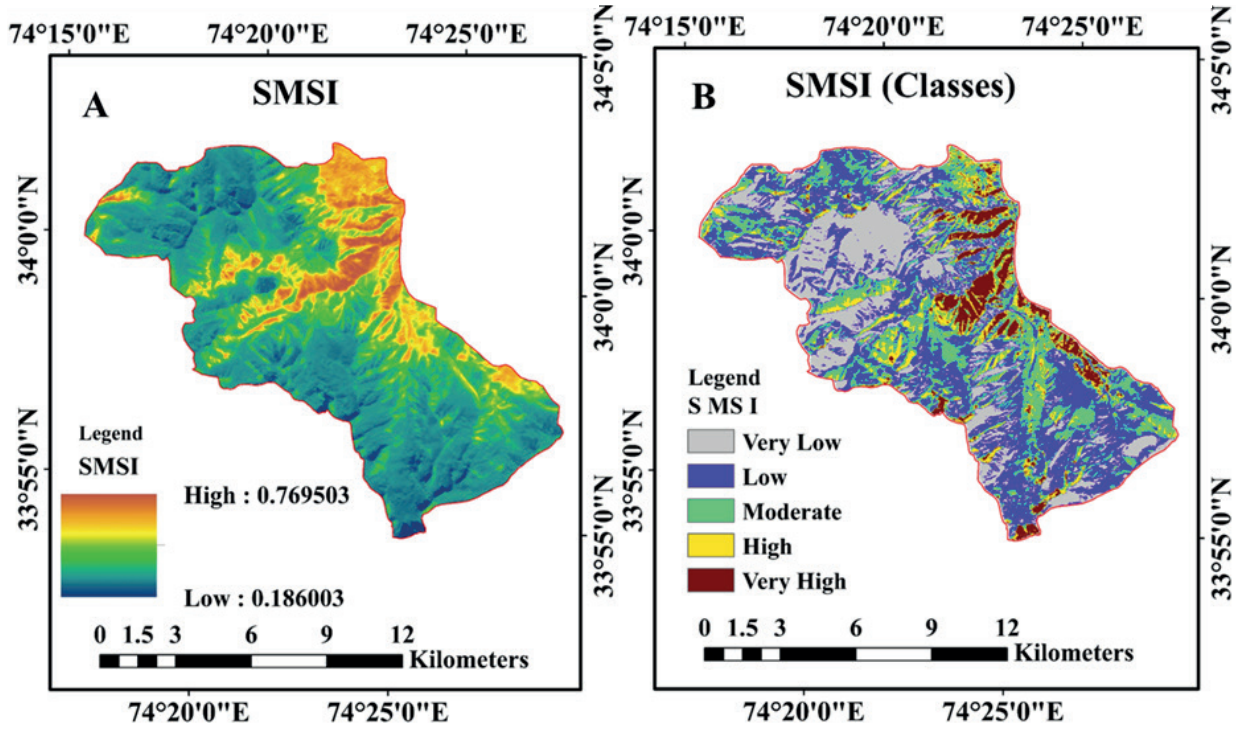

Fig. 10. Final SMSI Analysis A: Index, B: Classes

Citation: Bulletin of Geography. Physical Geography Series 2026, 31, http://doi.org/10.12775/bgeo-2026-0011

Table 8. Final SMSI of the Gulmarg region

SMSI class	Area [km²]	Area [%]	LST Range [°C]	Elevation [m]
Very low	1.12	0.86	<0	>4,000
Low	19.32	14.81	1–5.33	3,500–3,999
Moderate	88.40	67.79	5.34–7.57	3,000–3,499
High	16.24	12.45	7.58–11.23	2,501–2,999
Very high	5.34	4.09	>11	<2,500
Total	**130.42**	**100**	-	-

to incremental temperature increases, making them critical from a climate-change vulnerability perspective.

The low-sensitivity zone (14.81%), distributed between 3,500 m and 3,999 m, corresponds to relatively cooler temperature conditions ranging from 1°C to 5.33°C, where melt processes remain limited due to reduced thermal forcing. Above 4,000 m, the Very Low class occupies only 0.86% (1.12 km²) of the total area, reflecting persistent sub-zero LST (<0°C) and stable snowpack conditions. The small proportion of this class suggests that only a limited high-altitude core retains strong resistance to melt under present thermal conditions (Yadav et al. 2021). In contrast, the lower elevation zones exhibit intensified melt sensitivity. The high sensitivity class and the very high class extended over 12.45% and 4.09% area, respectively. Both are lies predominantly below 3,000 m, where LST exceeds 7.5°C, reaching above 12°C in the most vulnerable regions. These areas likely represent active melt corridors, possibly aligned with south-facing slopes, valley bottoms and thermally exposed terrain (Saloranta et al. 2019). Although they cover a smaller spatial extent compared to the moderate class, their contribution to seasonal runoff and snow depletion may be disproportionately high.

Critically, the class-wise distribution demonstrates a clear inverse relationship between elevation and melt sensitivity: as altitude decreases and surface temperature increases, melt intensity rises sharply (Shrestha et al. 2012). The dominance of the moderate class suggests that Gulmarg currently lies in a thermally responsive equilibrium state. However, the fact that nearly one sixth of the landscape is assigned to high to very high sensitivity categories indicates potential susceptibility to accelerated snow loss under continued warming. The minimal very-low area further emphasises that truly stable, cold snowpack zones are spatially restricted (Bothale et al. 2015). Overall, the SMSI classification confirms that snow melt sensitivity in Gulmarg is strongly thermally driven and elevation-moderated, with mid-elevation zones acting as the most climate-sensitive transition belt. This pattern highlights the importance of monitoring temperature trends and elevation-dependent melt responses for future hydrological and ecological stability in the region (Huang et al. 2016).

Relationship between SMSI, LST and Elevation

The correlation matrix illustrates the interrelationship among LST, Elevation and SMSI in the Gulmarg region, highlighting the dominant environmental controls governing snow melt dynamics (Fig. 11). The strongest relationship observed is between LST and SMSI (r=0.72), indicating a strong positive correlation. This suggests that melt sensitivity increases substantially with rising surface temperature, confirming that thermal forcing is the primary driver of snow melt processes in the region (Husain et al. 2022). Areas experiencing higher LST values correspond to higher SMSI values, reflecting intensified melt susceptibility under warmer surface conditions. A strong negative correlation exists between LST and Elevation (r=−0.66), demonstrating a clear

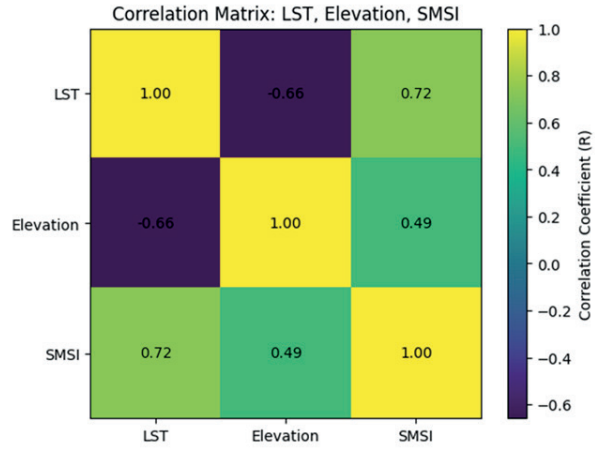

Fig. 11. Correlation between SMSI with LST and elevation

lapse-rate effect where temperature decreases with increasing altitude (Zhao et al. 2019). The magnitude of this correlation indicates that elevation significantly regulates the spatial variability of surface temperature (Prakash and Norouzi 2020). The relationship between Elevation and SMSI (r=0.49) shows a moderate positive association. Although melt energy generally decreases with altitude, higher elevations in the study area also contain more persistent snow reserves and larger areas of snow cover; when these zones show wetness or elevated LST, they can register as sensitive within the integrated SMSI. Therefore, elevation acts both as a cooling control and as a proxy for snow-storage potential, producing a positive but secondary association with SMSI (Yadav et al. 2021; Dimri et al. 2022). Nevertheless, the weaker magnitude compared to LST-SMSI suggests that elevation acts as a secondary control, which influences melt indirectly through its effect on temperature rather than directly driving melt intensity (Tiwari et al. 2016).

Overall, the figure confirms that snow melt sensitivity in Gulmarg is predominantly thermally driven, with strong topographic moderation through elevation-dependent temperature gradients. The clear hierarchical structure of correlations (LST-SMSI>LST-Elevation>Elevation-SMSI) supports the earlier PCA findings, where LST and elevation emerged as dominant contributors to melt variability. This integrated statistical evidence strengthens the conclusion that temperature is the principal melt driver, while terrain modulates its spatial expression across the landscape.

Conclusion and suggestions

This study successfully demonstrates a multispectral, temperature and topographic integrated geospatial framework for assessing snow melt sensitivity in the Gulmarg region of the Western Himalayas. By combining snow presence, snow moisture, snow wetness, land surface temperature and topographic elevation within a standardised and statistically weighted modelling structure, the SMSI provides a spatially explicit understanding of melt vulnerability across high-altitude terrain.

The snow cover extent analysis revealed that more than half of the total study area remained snow-covered during early February 2025, reflecting peak winter accumulation conditions. However, the thermal analysis indicated substantial heterogeneity, with LST ranging from −3.90°C to 12.92°C and a relatively high standard deviation (5.47°C), suggesting strong topographic and surface-condition controls. Elevation ranged from 2,331 m to 4,557 m, reinforcing the pronounced altitudinal gradient that governs both temperature distribution and snow persistence.

The PCA-based weighting approach proved critical in objectively identifying dominant melt drivers. The first principal component explained 55.77% of total variance, capturing the primary environmental gradient influencing snow melt. LST emerged as the most influential variable (24.7%), confirming that thermal forcing is the principal control of snow melt sensitivity. Elevation followed closely (23.9%), demonstrating that topography regulates melt primarily through temperature lapse-rate effects rather than independent control. The strong contribution of SWI (23.2%) and moderate role of NDSMI (15.6%) highlight the importance of internal snowpack wetness and moisture conditions in accelerating ablation processes. In contrast, NDSI (12.3%) and especially NDSCI (0.3%) contributed comparatively less to the dominant melt gradient, suggesting that snow presence alone is insufficient to explain melt sensitivity without integrating thermal and moisture dynamics.

The SMSI classification further clarifies spatial vulnerability patterns. Nearly 67.79% of the landscape falls under moderate melt sensitivity, primarily between 3,000 m and 3,499 m elevation. These mid-elevation zones represent transitional climatic belts that are neither thermally stable nor fully ablation-dominated. Such areas are particularly vulnerable to incremental warming and may shift rapidly toward higher melt classes under continued temperature rise. Approximately 16.54% of the area falls under high to very high sensitivity categories, predominantly below 3,000 m, where LST exceeds 7.5°C and reaches above 11°C in localised pockets. Although spatially limited, these zones likely contribute disproportionately to seasonal runoff generation and snow depletion.

Correlation analysis reinforces the hierarchical structure of environmental controls. The correlation between LST and SMSI confirms that snow melt sensitivity increases substantially with rising surface temperature. The negative correlation between LST and elevation reflects classic lapse-rate behaviour, while the moderate elevation-SMSI relationship indicates indirect topographic influence mediated through temperature gradients. Together with PCA findings, these relationships provide statistically consistent evidence that snow melt in Gulmarg is fundamentally thermally driven but topographically moderated.

From a broader climatic perspective, the observed upward temperature trend in Gulmarg (0.73°C per year over the last decade) is particularly alarming. The snowmelt contributes substantially to river basin discharge, and changes in the timing and intensity of melt can affect irrigation supply, hydropower scheduling, drinking-water availability and spring-summer low-flow conditions. High-sensitivity zones may contribute disproportionately to early runoff pulses, while rapid warming or rain-on-snow episodes can increase flood risk and compound hazards associated with avalanches, slope instability and glacial-lake outburst flood vulnerability in the wider Himalayan region. Water-resource managers should therefore combine SMSI-type spatial products with streamflow observations, snow-depth records and seasonal forecasts.

The methodological framework adopted in this study demonstrates several strengths. The integration of multi-spectral indices with LST and elevation enhances process-level interpretation beyond simple snow-cover mapping. Z-score normalisation ensures statistical comparability across variables measured in different units, while PCA provides an objective weight assignment mechanism free from subjective bias. The weighted overlay approach allows translation of complex statistical relationships into spatially interpretable vulnerability zones.

However, certain limitations remain. The analysis is based on a single-date winter observation and thus represents a snapshot of spatial sensitivity, not a temporal melt trajectory. Multi-temporal or seasonal datasets would strengthen temporal trend detection and improve dynamic modelling of melt progression. Additionally, incorporating meteorological ground observations such as snowfall depth, snow water equivalent or albedo measurements could further validate remote sensing-derived indices. Finally, slope, aspect, terrain shadowing and potential solar radiation were not explicitly incorporated, although they are important local controls on melt energy. Despite these limitations, the present SMSI framework provides a reproducible, policy-relevant and spatially explicit tool for identifying thermally sensitive snow zones in Gulmarg and can be adapted for other Himalayan basins to support climate adaptation, water-resource planning and sustainable mountain tourism.

In conclusion, this study confirms that snow melt sensitivity in Gulmarg is primarily controlled by land surface temperature, strongly influenced by elevation-dependent warming, and dynamically modulated by snow wetness and moisture conditions. The dominance of moderate sensitivity zones indicates that the region currently exists in a climatically responsive equilibrium state, yet the presence of expanding high-sensitivity areas suggests potential instability under future warming scenarios.

Disclosure statement

No potential conflict of interest was reported by the authors

Author contributions

Study design: AKD; data collection: AKD; statistical analysis: SS; result interpretation: AKD; manuscript preparation: SS; literature review: SS.

References

ABDI H and WILLIAMS LJ, 2010, Principal component analysis. *Wiley Interdisciplinary Reviews: Computational Statistics* 2(4): 433–459. DOI: https://doi.org/10.1002/wics.101.

ADEOLA FASHAE O, GBENGA ADAGBASA E, OLUDAPO OLUSOLA A and OLUSEYI OBATERU R, 2020, Land use/land cover change and land surface temperature of Ibadan and environs, Nigeria. *Environmental Monitoring and Assessment* 192(2). DOI: https://doi.org/10.1007/s10661-019-8054-3.

AKINKUNMI WB and ETEBEFIA SO, 2019, Use of Correlation, Tolerance and Variance Inflation Factor. *Global Scientific Journal* 7(5): 652–659.

AREKHI M, 2016, Analysis of spatial-temporal variation of land surface temperature, vegetation and snow cover in Lar National Park of Iran. *International Archives of the Photogrammetry, Remote Sensing and Spatial Information Sciences - ISPRS Archives* 42(2W1): 37–43. DOI: https://doi.org/10.5194/isprs-archives-XLII-2-W1-37-2016.

BABA MW, GASCOIN S, KINNARD C, MARCHANE A and HANICH L, 2019, Effect of Digital Elevation

Model Resolution on the Simulation of the Snow Cover Evolution in the High Atlas. *Water Resources Research* 55(7): 5360–5378. DOI: https://doi.org/10.1029/2018WR023789.

BHAT AA, DHONDIRAM PD, GUPTA SK, KANGA S, SINGH SK, MERAJ G, KUMAR P and SAJAN B, 2025, Snow Resources and Climatic Variability in Jammu and Kashmir, India. *Climate* 13(2): 28. DOI: https://doi.org/10.3390/cli13020028.

BLYTH S, 1994, Karl Pearson and the Correlation Curve. *International Statistical Review / Revue Internationale de Statistique* 62(3): 393–403.

BORMANN KJ, BROWN RD, DERKSEN C and PAINTER TH, 2018, Estimating snow-cover trends from space. *Nature Climate Change* 8(11): 924–928. DOI: https://doi.org/10.1038/s41558-018-0318-3.

BOTHALE RV, RAO PVN, DUTT CBS and DADHWAL VK, 2015, Detection of snow melt and freezing in Himalaya using OSCAT data. *Journal of Earth System Science* 124(1): 101–113. DOI: https://doi.org/10.1007/s12040-014-0524-y.

BRAHMBHATT RM, BAHUGUNA I, RATHORE BP, KULKARNI AV, SHAH RD, NAINWAL HC and AJAI, 2012, Variation of Snowline and Mass Balance of Glaciers of Warwan and Bhut Basins of Western Himalaya Using Remote Sensing Technique. *Journal of the Indian Society of Remote Sensing* 40(4): 629–637. DOI: https://doi.org/10.1007/s12524-011-0186-z.

BRO R and SMILDE AK, 2014, Principal component analysis. *Analytical Methods* 6(9): 2812–2831. DOI: https://doi.org/10.1039/c3ay41907j.

CHOATE MJ, RENGARAJAN R, STOREY JC and LUBKE M, 2023, Landsat 9 Geometric Commissioning Calibration Updates and System Performance Assessment. *Remote Sensing* 15(14). DOI: https://doi.org/10.3390/rs15143524.

CZAPLA-MYERS JS, THOME KJ, ANDERSON NJ, LEIGH LM, PINTO CT and WENNY BN, 2024, The Ground-Based Absolute Radiometric Calibration of the Landsat 9 Operational Land Imager. *Remote Sensing* 16(6). DOI: https://doi.org/10.3390/rs16061101.

DAR FA, RAMANATHAN A, MIR RA and PIR RA, 2024, Groundwater scenario under climate change and anthropogenic stress in Ladakh Himalaya, India. *Journal of Water and Climate Change* 15(4): 1459–1489. DOI: https://doi.org/10.2166/wcc.2024.307.

DAR RA, RASHID I, ROMSHOO SA and MARAZI A, 2014, Sustainability of winter tourism in a changing climate over Kashmir Himalaya. *Environmental Monitoring and Assessment* 186(4): 2549–2562. DOI: https://doi.org/10.1007/s10661-013-3559-7.

DESINAYAK N, PRASAD AK, EL-ASKARY H, KAFATOS M and ASRAR GR, 2022, Snow cover variability and trend over the Hindu Kush Himalayan region using MODIS and SRTM data. *Annales Geophysicae* 40(1): 67–82. DOI: https://doi.org/10.5194/angeo-40-67-2022.

DEVAKI H and SHANMUGAPRIYA S, 2023, Site suitability analysis for locating construction and demolition waste transfer station: an Indian case study. *Environmental Monitoring and Assessment* 195(9). DOI: https://doi.org/10.1007/s10661-023-11723-7.

DIMRI AP, PALAZZI E and DALOZ AS, 2022, Elevation dependent precipitation and temperature changes over Indian Himalayan region. *Climate Dynamics* 59(1–2): 1–21. DOI: https://doi.org/10.1007/s00382-021-06113-z.

DIXIT A, GOSWAMI A and JAIN S, 2019, Development and evaluation of a new "Snow Water Index (SWI)" for accurate snow cover delineation. *Remote Sensing* 11(23). DOI: https://doi.org/10.3390/rs11232774.

DUBEY AK, RIZVI FF and TIWARI A, 2025, Gauging land surface temperatures with changes in land use land cover: a spatiotemporal analysis of Gaya City, Bihar. *Singapore Journal of Tropical Geography* 46(3): 386–409. DOI: https://doi.org/10.1111/sjtg.70019.

DWIVEDI CS, KUMARI S, PANDEY AC, PARIDA BR and SIKKA G, 2024, Site Suitability Analysis of a Municipal Solid Waste Management System in Ranchi City Using AHP: A Multi-Criteria Decision Approach. *Environmental Quality Management* 34(1): 1–15. DOI: https://doi.org/10.1002/tqem.22312.

GARG S, SINGH KK, SIDHU BS and MISHRA VD, 2014, Monitoring and Analysis of North-West Himalayan Snow Cover using Optical Satellite Data and In-Situ Observations. *International Journal of Engineering Research & Technology* 3(8): 218–224.

GROSS G, HELDER D, BEGEMAN C, LEIGH L, KAEWMANEE M and SHAH R, 2022, Initial Cross-Calibration of Landsat 8 and Landsat 9 Using the Simultaneous Underfly Event. *Remote Sensing* 14(10). DOI: https://doi.org/10.3390/rs14102418.

GROVER A and SINGH RB, 2016, Monitoring Spatial patterns of land surface temperature and urban heat island for sustainable megacity: A case study of Mumbai, India, using landsat TM data. *Environment*

and Urbanization ASIA 7(1): 38–54. DOI: https://doi.org/10.1177/0975425315619722.

GUHA S, GOVIL H and DIWAN P, 2020, Monitoring LST-NDVI Relationship Using Premonsoon Landsat Datasets. *Advances in Meteorology* 2020(1). DOI: https://doi.org/10.1155/2020/4539684.

GURUNG DR, MAHARJAN SB, SHRESTHA AB, SHRESTHA MS, BAJRACHARYA SR and MURTHY MSR, 2017, Climate and topographic controls on snow cover dynamics in the Hindu Kush Himalaya. *International Journal of Climatology* 37(10): 3873–3882. DOI: https://doi.org/10.1002/joc.4961.

HAQ MA, BARAL P, YARAGAL S and RAHAMAN G, 2020, Assessment of trends of land surface vegetation distribution, snow cover and temperature over entire Himachal Pradesh using MODIS datasets. *Natural Resource Modeling* 33(2). DOI: https://doi.org/10.1111/nrm.12262.

HUANG X, DENG J, MA X, WANG Y, FENG Q, HAO X and LIANG T, 2016, Spatiotemporal dynamics of snow cover based on multi-source remote sensing data in China. *Cryosphere* 10(5): 2453–2463. DOI: https://doi.org/10.5194/tc-10-2453-2016.

HUSAIN MA, KUMAR P, SINGH A, RAMAN VAV, DUA R and THAKUR S, 2022, Snow Cover and Snowline Variation in Relation to Land Surface Temperature in Spiti Valley, Himachal Pradesh, India. *International Journal of Ecology and Environmental Sciences* 49(2): 187–199. DOI: https://doi.org/10.55863/ijees.2023.2624.

JEELANI G, FEDDEMA JJ, VAN DER VEEN CJ and STEARNS L, 2012, Role of snow and glacier melt in controlling river hydrology in Liddar watershed (western Himalaya) under current and future climate. *Water Resources Research* 48(12). DOI: https://doi.org/10.1029/2011WR011590.

JOSHI R, KUMAR K, PANDIT J and PALNI LMS, 2015, Variations in the Seasonal Snow Cover Area (SCA) for Upper Bhagirathi Basin, India: 9–21. DOI: https://doi.org/10.1007/978-3-319-13743-8_2.

KARIMI H, AMIRI S, HUANG J and KARIMI A, 2019, Integrating GIS and multi-criteria decision analysis for landfill site selection, case study: Javanrood County in Iran. *International Journal of Environmental Science and Technology* 16(11): 7305–7318. DOI: https://doi.org/10.1007/s13762-018-2151-7.

KULKARNI AV, BAHUGUNA IM, RATHORE BP, SINGH SK, RANDHAWA SS, SOOD RK and DHAR S, 2007, Glacial retreat in Himalaya using Indian Remote Sensing satellite data. *Current Science* 92(1): 69–74. DOI: https://doi.org/10.1117/12.694004.

LI H, LIU J, LEI X, JU Y, BU X and LI H, 2022, Quantitative determination of environmental factors governing the snow melting: a geodetector case study in the central Tienshan Mountains. *Scientific Reports* 12(1): 11565. DOI: https://doi.org/10.1038/s41598-022-15722-5.

MA Y and ZHANG Y, 2022, IMPROVED ON SNOW COVER EXTRACTION IN MOUNTAINOUS AREAS BASED ON MULTI-FACTOR NDSI DYNAMIC THRESHOLD. *The International Archives of the Photogrammetry, Remote Sensing and Spatial Information Sciences* XLIII-B3-2: 771–778. DOI: https://doi.org/10.5194/isprs-archives-XLIII-B3-2022-771-2022.

MALIK MS, SHUKLA JP and MISHRA S, 2019, Relationship of LST, NDBI and NDVI using Landsat-8 data in Kandaihimmat. *Indian Journal of Geo Marine Sciences* 48(01): 25–31.

MISHRA AK and RAFIQ M, 2017, Analyzing snowfall variability over two locations in Kashmir, India in the context of warming climate. *Dynamics of Atmospheres and Oceans* 79: 1–9. DOI: https://doi.org/10.1016/j.dynatmoce.2017.05.002.

MISRA A, KUMAR A, BHAMBRI R, HARITASHYA UK, VERMA A, DOBHAL DP, GUPTA AK, GUPTA G and UPADHYAY R, 2020, Topographic and climatic influence on seasonal snow cover: Implications for the hydrology of ungauged Himalayan basins, India. *Journal of Hydrology* 585(February). DOI: https://doi.org/10.1016/j.jhydrol.2020.124716.

MUDRYK LR, KUSHNER PJ, DERKSEN C and THACKERAY C, 2017, Snow cover response to temperature in observational and climate model ensembles. *Geophysical Research Letters* 44(2): 919–926. DOI: https://doi.org/10.1002/2016GL071789.

NEGI HS, THAKUR NK, KUMAR R and KUMAR M, 2009, Monitoring and evaluation of seasonal snow cover in Kashmir valley using remote sensing, GIS and ancillary data. *Journal of Earth System Science* 118(6): 711–720. DOI: https://doi.org/10.1007/s12040-009-0057-y.

NOTARNICOLA C, 2022, Overall negative trends for snow cover extent and duration in global mountain regions over 1982–2020. *Scientific Reports* 12(1): 13731. DOI: https://doi.org/10.1038/s41598-022-16743-w.

OLUSINA JO and SHYLLON DO, 2014, Suitability Analysis in Determining Optimal Landfill Location

Using Multi-Criteria Evaluation (MCE), GIS & Remote Sensing. *Int J Comput Eng Res* 4(6): 7–20.

OPARIN VN, POTAPOV VP, GINIYATULLINA OL, ANDREEVA NV, SCHASTLIVTSEV EL and BYKOV AA, 2014, Evaluation of dust pollution of air in Kuzbass coal-mining areas in winter by data of remote earth sensing. *Journal of Mining Science* 50(3): 549–558. DOI: https://doi.org/10.1134/S1062739114030168.

OYEDELE AA, OMOSEKEJI AE, AYENI OO, EWUMI TO and OGUNLANA FO, 2022, Delineation of Landfill Sites for Municipal Solid Waste Management using GIS. *Journal of Human, Earth, and Future* 3(3): 321–332. DOI: https://doi.org/10.28991/HEF-2022-03-03-05.

ÖZKAN B, ÖZCEYLAN E and SARIÇIÇEK İ, 2019, GIS-based MCDM modeling for landfill site suitability analysis: A comprehensive review of the literature. *Environmental Science and Pollution Research* 26(30): 30711–30730. DOI: https://doi.org/10.1007/s11356-019-06298-1.

PANAHI M, RESOURCES M and REZAIE F, 2013, The Relationship between NDVI and LST in the urban area of Mashhad, Iran. *International Conference on Civil Engineering Architecture & Urban Sustainable Development*.

POTOPOVÁ V, BORONEANȚ C, MOŽNÝ M and SOUKUP J, 2016, Driving role of snow cover on soil moisture and drought development during the growing season in the Czech Republic. *International Journal of Climatology* 36(11): 3741–3758. DOI: https://doi.org/10.1002/joc.4588.

POUSSIN C, TIMONER P, CHATENOUX B, GIULIANI G and PEDUZZI P, 2023, Improved Landsat-based snow cover mapping accuracy using a spatiotemporal NDSI and generalized linear mixed model. *Science of Remote Sensing* 7(February): 100078. DOI: https://doi.org/10.1016/j.srs.2023.100078.

PRAKASH S and NOROUZI H, 2020, Land surface temperature variability across India: a remote sensing satellite perspective. *Theoretical and Applied Climatology* 139(1–2): 773–784. DOI: https://doi.org/10.1007/s00704-019-03010-8.

RAFIQ M, PARA JA, KESARKAR AP and LOTUS S, 2021, A study of extreme snowfall during 2019 and 2020 across the Kashmir Himalaya. *Weather* 76(10): 333–337. DOI: https://doi.org/10.1002/wea.3938.

RAGHUBANSHI S, AGRAWAL R and RATHORE BP, 2023, Enhanced snow cover mapping using object-based classification and normalized difference snow index (NDSI). *Earth Science Informatics* 16(3): 2813–2824. DOI: https://doi.org/10.1007/s12145-023-01077-6.

RANI KMR, DUBEY AK and ANJUM M, 2025, Impact assessment of the adaptation of modernization to the Indian agrarian society: Empirical evidence from the Haraiya Block of Azamgarh District, Uttar Pradesh. *Irrigation and Drainage* 74(1): 389–401. DOI: https://doi.org/10.1002/ird.2999.

RASUL A and NINGTHOUJAM R, 2021, Snow cover and vegetation greenness with leaf water content control the global land surface temperature. *Environment, Development and Sustainability* 23(10): 14722–14748. DOI: https://doi.org/10.1007/s10668-021-01269-4.

RINGNÉR M, 2008, What is principal component analysis? *Nature Biotechnology* 26(3): 303–304. DOI: https://doi.org/10.1038/nbt0308-303.

ROMSHOO SA, RAFIQ M and RASHID I, 2014, Mohammd-Rafiq Estimation and validation of Remotely Sensed Land Surface Temperature in Kashmir Valley. *Journal of Himalayan Ecology & Sustainable Development* 9(May).

SALOMONSON V and APPEL I, 2004, Estimating fractional snow cover from MODIS using the normalized difference snow index. *Remote Sensing of Environment* 89(3): 351–360. DOI: https://doi.org/10.1016/j.rse.2003.10.016.

SALORANTA T, THAPA A, KIRKHAM JD, KOCH I, MELVOLD K, STIGTER E, LITT M and MØEN K, 2019, A Model Setup for Mapping Snow Conditions in High-Mountain Himalaya. *Frontiers in Earth Science* 7. DOI: https://doi.org/10.3389/feart.2019.00129.

SAM SC and BALASUBRAMANIAN G, 2023, Spatiotemporal detection of land use/land cover changes and land surface temperature using Landsat and MODIS data across the coastal Kanyakumari district, India. *Geodesy and Geodynamics* 14(2): 172–181. DOI: https://doi.org/10.1016/j.geog.2022.09.002.

SATTI Z, NAVEED M, SHAFEEQUE M, ALI S, ABDULLAEV F, ASHRAF TM, IRSHAD M and LI L, 2023, Effects of climate change on vegetation and snow cover area in Gilgit Baltistan using MODIS data. *Environmental Science and Pollution Research* 30(7): 19149–19166. DOI: https://doi.org/10.1007/s11356-022-23445-3.

SHAFIQ M UL, AHMED P, ISLAM Z UL, JOSHI PK and BHAT WA, 2019, Snow cover area change and its relations with climatic variability in Kashmir Himalayas, India. *Geocarto International* 34(6): 688–

702. DOI: https://doi.org/10.1080/10106049.2018.1469675.

SHARMA V, MISHRA VD and JOSHI PK, 2012, Snow cover variation and streamflow simulation in a snow-fed river basin of the Northwest Himalaya. *Journal of Mountain Science* 9(6): 853–868. DOI: https://doi.org/10.1007/s11629-012-2419-1.

SHRESTHA M, WANG L, KOIKE T, XUE Y and HIRABAYASHI Y, 2012, Modeling the Spatial Distribution of Snow Cover in the Dudhkoshi Region of the Nepal Himalayas. *Journal of Hydrometeorology* 13(1): 204–222. DOI: https://doi.org/10.1175/JHM-D-10-05027.1.

SHRESTHA N, 2021, Factor Analysis as a Tool for Survey Analysis. *American Journal of Applied Mathematics and Statistics* 9(1): 4–11. DOI: https://doi.org/10.12691/ajams-9-1-2.

SINGH A, ORGANISATION D, KUMAR S and STUDIES E, 2012, ON THE SNOWPACK VARIABILITY IN GULMARG REGION OF INDIAN HIMALAYA. Snow and Avalanche Study Establishment, December.

SINHA S, DUBEY AK, RAJ S and MOHAPATRA S, 2025, Shrinking Snow Cover and Its Implications for Ski in Gulmarg: A Case Study of International Athletes. *International Journal of Human Movement and Sports Sciences* 13(2): 366–380. DOI: https://doi.org/10.13189/saj.2025.130214.

STEGER C, KOTLARSKI S, JONAS T and SCHÄR C, 2013, Alpine snow cover in a changing climate: a regional climate model perspective. *Climate Dynamics* 41(3–4): 735–754. DOI: https://doi.org/10.1007/s00382-012-1545-3.

STEIGER R, SCOTT D, ABEGG B, PONS M and AALL C, 2019, A critical review of climate change risk for ski tourism. *Current Issues in Tourism* 22(11): 1343–1379. DOI: https://doi.org/10.1080/13683500.2017.1410110.

STIGTER EE, WANDERS N, SALORANTA TM, SHEA JM, BIERKENS MFP and IMMERZEEL WW, 2016, Climate sensitivity of snow water equivalent and snowmelt runoff in a Himalayan catchment. DOI: https://doi.org/10.5194/tc-2016-216.

STILLINGER T, RITTGER K, RALEIGH MS, MICHELL A, DAVIS RE and BAIR EH, 2023, Landsat, MODIS, and VIIRS snow cover mapping algorithm performance as validated by airborne lidar datasets. *The Cryosphere* 17(2): 567–590. DOI: https://doi.org/10.5194/tc-17-567-2023.

TAYLOR LS, QUINCEY DJ, SMITH MW, BAUMHOER CA, MCMILLAN M and MANSELL DT, 2021, Remote sensing of the mountain cryosphere: Current capabilities and future opportunities for research. *Progress in Physical Geography: Earth and Environment* 45(6): 931–964. DOI: https://doi.org/10.1177/03091333211023690.

THIEBAULT K and YOUNG S, 2020, Snow cover change and its relationship with land surface temperature and vegetation in northeastern North America from 2000 to 2017. *International Journal of Remote Sensing* 41(21): 8453–8474. DOI: https://doi.org/10.1080/01431161.2020.1779379.

TIAN L, ZHANG B and WU P, 2022, A global drought dataset of standardized moisture anomaly index incorporating snow dynamics (SZIsnow) and its application in identifying large-scale drought events. *Earth System Science Data* 14(5): 2259–2278. DOI: https://doi.org/10.5194/essd-14-2259-2022.

TIWARI S, KAR SC and BHATLA R, 2016, Examination of snowmelt over Western Himalayas using remote sensing data. *Theoretical and Applied Climatology* 125(1–2): 227–239. DOI: https://doi.org/10.1007/s00704-015-1506-y.

TREVISIOL F, MANDANICI E, PAGLIARANI A and BITELLI G, 2024, Evaluation of Landsat-9 interoperability with Sentinel-2 and Landsat-8 over Europe and local comparison with field surveys. *ISPRS Journal of Photogrammetry and Remote Sensing* 210(February): 55–68. DOI: https://doi.org/10.1016/j.isprsjprs.2024.02.021.

VARADE D and DIKSHIT O, 2020, Assessment of winter season land surface temperature in the Himalayan regions around the Kullu area in India using landsat-8 data. In: *Geocarto International* 35(6). DOI: https://doi.org/10.1080/10106049.2018.1520928.

VINZE P and AZAM MF, 2023, On the transferability of snowmelt runoff model parameters: Discharge modeling in the Chandra-Bhaga Basin, western Himalaya. *Frontiers in Water* 4. DOI: https://doi.org/10.3389/frwa.2022.1086557.

VOSKANIAN N, THOME K, WENNY BN, TAHERSIMA MH and YARAHMADI M, 2023, Combining RadCalNet Sites for Radiometric Cross Calibration of Landsat 9 and Landsat 8 Operational Land Imagers (OLIs). *Remote Sensing* 15(24). DOI: https://doi.org/10.3390/rs15245752.

WANG X, JIA K, LIANG S, LI Q, WEI X, YAO Y, ZHANG X and TU Y, 2017, Estimating Fractional

Vegetation Cover from Landsat-7 ETM+ Reflectance Data Based on a Coupled Radiative Transfer and Crop Growth Model. *IEEE Transactions on Geoscience and Remote Sensing* 55(10): 5539–5546. DOI: https://doi.org/10.1109/TGRS.2017.2709803.

XU W, MA L, MA M, ZHANG H and YUAN W, 2017, Spatial-temporal variability of snow cover and depth in the Qinghai-Tibetan plateau. *Journal of Climate* 30(4): 1521–1533. DOI: https://doi.org/10.1175/JCLI-D-15-0732.1.

YADAV JS, MISRA A, DOBHAL DP, YADAV RBS and UPADHYAY R, 2021, Snow cover mapping, topographic controls and integration of meteorological data sets in Din-Gad Basin, Central Himalaya. *Quaternary International* 575–576: 160–177. DOI: https://doi.org/10.1016/j.quaint.2020.05.030.

YADAV JS, TIWARI SK, MISRA A, RAI SK and YADAV RK, 2021, High-altitude meteorology of Indian Himalayan Region: complexities, effects, and resolutions. *Environmental Monitoring and Assessment* 193(10): 654. DOI: https://doi.org/10.1007/s10661-021-09418-y.

YIN F, LEWIS PE and GÓMEZ-DANS JL, 2022, Bayesian atmospheric correction over land: Sentinel-2/MSI and Landsat 8/OLI. *Geoscientific Model Development* 15(21): 7933–7976. DOI: https://doi.org/10.5194/gmd-15-7933-2022.

YOUNG SS, 2023, Global and Regional Snow Cover Decline: 2000–2022. *Climate* 11(8): 162. DOI: https://doi.org/10.3390/cli11080162.

ZAZ SN, AHMAD RS, KRISHNAMOORTHY RT and VISWANADHAPALLI YB, 2018, Climatic and extreme weather variations over Mountainous Jammu and Kashmir, India: Physical explanations based on observations and modelling. *Atmospheric Chemistry and Physics Discussions* 2: 1–36.

ZHAO W, HE J, WU Y, XIONG D, WEN F and LI A, 2019, An Analysis of Land Surface Temperature Trends in the Central Himalayan Region Based on MODIS Products. *Remote Sensing* 11(8): 900. DOI: https://doi.org/10.3390/rs11080900.

Received 28 February 2026
Accepted 2 June 2026